LANGMUIR

pubs.acs.org/Langmuir Article

Achieving Superhydrophobic Surfaces via Air-Assisted Electrospray

Thu Nguyen, Philip Wortman, Zizhou He, Joshua Goulas, Hui Yan, Mehdi Mokhtari, Xiao-Dong Zhou, and Ling Fei*

Cite This: *Langmuir* 2022, 38, 2852−2861 Read Online

ACCESS | Metrics & More | Article Recommendations

ABSTRACT: Superhydrophobic surface is an enabling technology in numerous emerging and practical applications such as self-cleaning, anticorrosion, antifouling, anti-icing coatings, and oil−water separation. Here, we report a facile air-assisted electrospray approach to achieve a superhydrophobic surface by systematically studying spray conditions and the chemistry of a coating precursor solution consisting of silicon dioxide nanoparticles, polyacrylonitrile, and *N*,*N*-dimethylformamide. The wettability behavior of the surface was analyzed with contact angle measurement and correlated with surface structures. The superhydrophobic coating exhibits remarkable water and oil repellent characteristics, as well as good robustness against abrasion and harsh chemical conditions. This air-assisted electrospray technique has shown great control over the coating process and properties and thus can be potentially used for various advanced industrial applications for self-cleaning and anticorrosion surfaces.

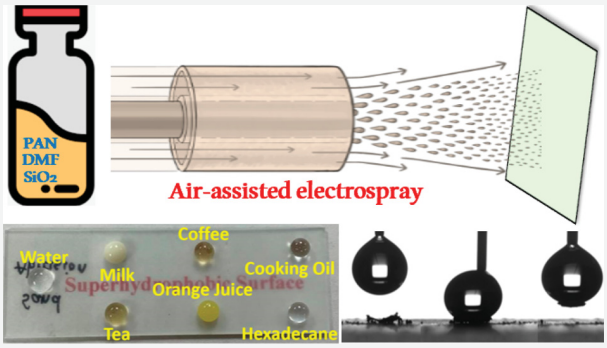

1. INTRODUCTION

In recent decades, self-cleaning materials have attracted growing attention in both academic research and industrial development, due largely to the inspiration by many biological surfaces in nature, such as lotus leaves, rose petals, butterfly wings, and desert beetles. Achieving a superhydrophobic surface thus has received the utmost attention to accommodate such development. These superhydrophobic surfaces exhibit a combination of micro/nano hierarchical roughness and low surface energy, which result in the special water repellency behavior.[1−4] Superhydrophobic surfaces have contact angles exceeding 150° in water basis.[5] The water droplets can easily roll off the superhydrophobic surface due to the low contact energy between solid and liquid. Therefore, these surfaces obtain a variety of novel functionalities consisting of antifouling, oil−water separation, anti-icing, antibacterial, self-cleaning, antigraffiti, and various other areas.[6−11]

Researchers have proposed various approaches to fabricate superhydrophobic coatings, including dip coating,[12] electrospinning,[13] thermal oxidation,[14] chemical vapor deposition,[15] spraying,[16,17] plasma and chemical etching,[18] sol−gel,[19,20] lithography,[21] and spin coating.[15] Conventional air gun spraying is one of the popular approaches to deposit the superhydrophobic coating on a variety of substrates. Recently, Zhu et al. demonstrated a method of spraying carbon nanotubes and silicon dioxide suspension onto glass slides.[20] After thermal treatment and surface fluorination, a transparent superamphiphobic coating was formed. Superamphiphobic surfaces exhibit static contact angles greater than 150° for both polar and nonpolar liquids.[22] This approach of spraying onto a small glass slide (approximately 8 × 2.5 cm) required a large amount of chemical solvent. For instance, 0.1 g of carbon nanotubes was dispersed in a 130 mL mixture of tetraethyl orthosilicate and ethanol (volume ratio 1:25). Namely, the spray precursor solutions are very dilute and only volatile solvent can be used, due to the requirement of solvent evaporation in the coating process. Similarly, Chen et al. fabricated a superhydrophobic coating on both hard and soft substrates via a conventional spraying method.[23] The coating was achieved by repeated spraying of adhesive followed by silicon dioxide for up to 10 cycles. Many of these conventional spraying approaches successfully produce superhydrophobic surfaces with an excellent self-cleaning performance and sufficient mechanical robustness against harsh environmental conditions. However, those procedures involve a large amount of volatile solvent or a time-consuming process.

To address these challenging problems while maintaining self-cleaning capacity, a simple air-assisted electrospray technique is used in this study to fabricate a superhydrophobic coating with good process control and coating properties. The air-assisted electrospray technique has a flexibility in the

Received: November 22, 2021
Revised: February 14, 2022
Published: February 22, 2022

https://doi.org/10.1021/acs.langmuir.1c03134
Langmuir 2022, 38, 2852−2861

precursor concentration or solvent volatility. This technique was inspired by the widely applied electrospinning method, thus possessing all the advantages that electrospinning has such as low cost, easy scale-up, and simultaneous solvent evaporation. It has been used in different types of electrode preparation, such as battery, supercapacitor, fuel cell, and solar cell.[24,25] Recently, the air-assisted electrospray approach has been used successfully to achieve superhydrophobic surfaces. Heo et al. prepared a superhydrophobic polytetrafluoroethylene nanoparticle surface with excellent scale-up application in the bag filter industry via the air-assisted electrospray method.[26] Niknejad et al. recently reported the fabrication of dual-layer nanofibrous polyacrylonitrile (PAN)/styrene−acrylonitrile (SAN) membrane and polystyrene microbead reinforced membranes using the air-assisted electrospraying process, thereby significantly reducing the pore wetting and permeation problems of the membrane distillation process.[27] The unique advantage of this approach is to form a coating layer with excellent adhesion and high uniformity in a timely manner.[28] The solvent quickly evaporates, resulting in a dry coating layer instantly during the spraying process.[24] Hence, this instantly drying spray process eliminates the possibility of cracking due to surface tension from solvent evaporation which is sometimes seen in conventional coating methods, such as dip coating or blading. The air-assisted electrospray technique is relatively straightforward and easy to scale up. In view of this, an effort to broaden the application prospects of superhydrophobicity on transparent surfaces via the air-assisted electrospray method was targeted in this paper with cost-effective materials and advanced self-cleaning capacity.

In this work, a mixture of silicon dioxide nanopowders and polyacrylonitrile/*N*,*N*-dimethylformamide solution was used to test the new method and assess its potential for surface coating applications. The process parameters involved including concentration, air flow rate, solution infused rate, and power voltage were thoroughly investigated. Further, different methods such as blading and dip coating were demonstrated for a better comparison of the quality and water repellent behavior of coatings. The wettability behavior of the surfaces was analyzed with contact angle measurement and correlated with the surface structures. A series of tests consisting of sandpaper abrasion, tape adhesion, antiacid/antibase, and outdoor exposure were conducted to examine the reliability of the coating against harsh environmental conditions. The results of this study could lead to potential uses in various industrial applications of self-cleaning and anticorrosion surfaces.

2. MATERIALS AND METHODS

2.1. Materials. Microscope glass slides (high-quality soda-lime glass, 3 in. × 1 in., with ground edges and frosted on one end, 90° corners) were acquired from Karter Scientific. Polyacrylonitrile (PAN; with average M_w = 150 000), silicon dioxide (SiO_2; spherical porous nanopowder, 5−20 nm particle size, 99.5% trace metals basis), and trichloro(1*H*,1*H*,2*H*,2*H*-perfluorooctyl)silane (97%) were sourced from Sigma-Aldrich Corp. (St. Louis, MO). *N*,*N*-Dimethylformamide (DMF), acetone (ACS reagent, ≥99.5%), and ethanol (96%, anhydrous) were purchased from VWR Chemicals. Carbon black (C65) was provided by Gelon Lib Group. Hydrochloric acid solution (1 M HCl) and sodium hydroxide solution (1 M NaOH) were obtained from Sigma-Aldrich. All chemicals were used without further purification. Deionized (DI) water purified in an ultrapure water system was used in all experiments.

2.2. Preparation of Superhydrophobic Coatings. The spraying solution was prepared by first adding a predetermined amount of PAN (varying from 0 mg to 200 mg) in 5 mL of DMF and then storing it in an oven overnight at 70 °C to obtain the PAN−DMF solution. SiO_2 nanoparticles were dispersed in PAN−DMF solution at room temperature with different concentrations ranging from 50 to 300 mg. The solution was then ultrasonicated for 3 h and stirred magnetically with a constant speed of 400 rpm for 24 h. Glass substrates were washed with ethanol, acetone, and deionized water at least three times. They were then ultrasonicated for 30 min and dried at room conditions for 2 h prior to coating on the substrates.

The prepared solution was deposited on the cleaned glass slides via the electrospray method at different voltages (range from 0 to 20 kV) under room conditions. Coaxial needles were used for electrospraying, where the solution was introduced through the inner needle (17 gauge) and air was injected to the outer needle at flow rates of 2, 3, 4, 5, and 6 L/min. The solution infused rates (10, 20, 30, 40, and 50 μL/min) and spray periods (0.25, 0.5, 0.75, 1, 1.5, 2, and 2.5 h) were set at predetermined values for different samples which were later characterized and optimized. A Walfront LZQ-7 acrylic air flowmeter was used to control the air flow rates.

Coated glass substrates were stored overnight at room temperature. They were annealed in air at 600 °C for 90 min and then modified with low surface energy trichloro(1*H*,1*H*,2*H*,2*H*-perfluorooctyl)silane via the chemical vapor deposition technique. The coated glass slides and an open glass vessel containing 40 μL of trichloro(1*H*,1*H*,2*H*,2*H*-perfluorooctyl)silane were placed in a homemade sealed pot for 5 min at a high vacuum condition and at room temperature. Afterward, the open glass vessel was then removed from the sealed pot, and the coated substrates themselves were sealed in the pot for 30 min at 80 °C to remove untreated silane residues.

2.3. Characterizations and Measurements. *2.3.1. Wetting Test.* A drop shape analyzer DSA 100 apparatus from KRUSS Co., Ltd., Germany, was used to measure the static water contact angle (WCA) of the coating at various air flow rates (2, 3, 4, 5, and 6 L/min). Water droplets with volumes of 2−3 μL consistently were deposited on the coated substrates. Static images of the droplets on the surfaces were captured and WCA data was collected by the apparatus. Contact angle measurements were taken at standard temperature and pressure.

2.3.2. Surface Morphology. Scanning electron microscopy (SEM; Scios 2 DualBeam) was used to investigate the morphologies and the thicknesses of the superhydrophobic coatings. Before generation of images captured by SEM, all samples were gold-sputtered under high vacuum condition with a sputter coater to improve the electrical conductivity of the coatings.

2.3.3. Transparency. The transparency of the most superhydrophobic surface was measured with the ultraviolet−visible (UV−vis) transmittance spectrum (Agilent Technologies). Air was used as the blank. The percentage of transmittance over the wavelength range 200−800 nm of the origin pristine glass slide versus the coated surface were obtained from the UV−vis apparatus.

2.3.4. Self-Cleaning Examination. The self-cleaning functionality of the coatings was experimented on with carbon black particles sprinkled on the sample's surface. The substrate was placed at an angle of 20° to the flat table surface. Deionized water was continuously injected to the surface. The self-cleaning capability was tested on the basis of the ability of water droplets to rinse off the surface with carbon black particles. Additionally, the experiment of a water droplet picking up carbon black particles on the coated surface was performed. Black and white images and videos of the self-cleaning examination were also captured with the drop shape analyzer DSA 100 apparatus.

2.3.5. Durability of Coated Layers. To assess durability, sandpaper abrasion, a tape adhesion test, an antiacid/antibase test, and outdoor exposure examination were performed.

2.3.5.1. Sand Abrasion Test. Sandpaper of grit 400 was used for the abrasion analysis. The coated glass slides were placed facedown onto the surface. A 100 g glass vessel of sand was placed on top of the coated substrates. The substrates were reciprocally moved with a

https://doi.org/10.1021/acs.langmuir.1c03134
Langmuir 2022, 38, 2852−2861

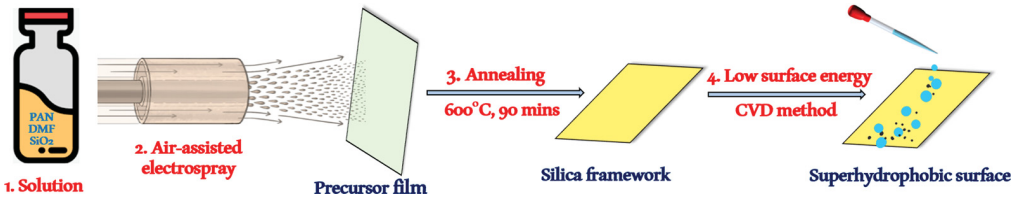

Figure 1. Schematic diagram of the fabrication process of superhydrophobic surface on glass substrate.

round trip distance of 10 cm. The round trip was referred to as one abrasion cycle. The WCA measurements of the coating before and after abrasion cycles were obtained for analysis.

2.3.5.2. Tape Adhesion Test. A 3M double-sided tape was used to perform the adhesion test. The coated glass slide was stably placed on an aluminum sheet with the coating surface facing up. The tape was attached to the coated surface, scratched, and then peeled off, which was referred to as one cycle. WCA measurements were performed before and after peeling cycles to evaluate the superhydrophobic property of the coatings.

2.3.5.3. Antiacid/Antibase Test. Two coated glass slides were separately immersed into two beakers containing 150 mL 1 M HCl and 1 M NaOH overnight. Afterward, the coated glass slides were dried in air under room conditions for 1 day. WCA measurements of the coated surface before and after immersion in acid and base solution were obtained. An additional experiment to rinse off the coated surface with DI water after the acid/base tests followed by drying in air at room temperature was conducted as well.

2.3.5.4. Outdoor Exposure Test. The coated glass slide was placed outside for 15 days, and a static water contact angle measurement was obtained every 3 days for analysis.

3. RESULTS AND DISCUSSION

In this work, superhydrophobic surfaces were obtained via air-assisted electrospraying, followed by thermal treatment and chemical vapor deposition (CVD) techniques as shown in Figure 1. The air-assisted electrospray tends to accelerate the drying of the deposition process by utilizing a convective air flow jet. The nozzle is comprised of two concentric cylindrical needles. The silicon dioxide (SiO_2) nanopowders in the polyacrylonitrile and dimethylformamide (PAN−DMF) solution were deposited to the substrate through the inner needle with the assistance of air through the outer needle for the air-assisted electrospray process. To be specific, the air helps atomize the big solution droplets into small ones so that electrostatic force is able to bring them to the target. Similar to electrospinning, solvent can be simultaneously evaporated during the process. This electrospray process is carried out at a high voltage condition. Using this method for electrode preparation, Halim et al. indicated that the dry solute is deposited on the substrate because smaller charged droplets are formed and solvent is evaporated faster via the assisting of the impinging dry air.[29] Wet solutions formed on the substrate may disrupt the uniformity with a low evaporation rate as the solute may migrate and agglomerate on the substrate upon solvent evaporation, whereas solute may form a discontinuity and disorder of the deposited materials with a fast evaporation rate.[29] To achieve the optimal evaporation rate during the air-assisted electrospraying process so that good control of structure is obtained, different parameters consisting of the power supply voltage, sprayed time, solution infused rate, and air flow rate are examined in this study. In addition, a variety of PAN and SiO_2 concentrations in DMF solution are tested to determine the effect of the sprayed solution on the superhydrophobic property of the coating. Thermal treatment and chemical vapor deposition steps are indicated in Figure 1 with corresponding conditions remaining unchanged for all testing samples.

3.1. Method Comparison. For comparison, dip coating and blading coating were also examined with the same precursor solution used in the electrospray. The static water contact angles of the coatings through the three methods are shown in Figure 2. The air-assisted electrospray method results

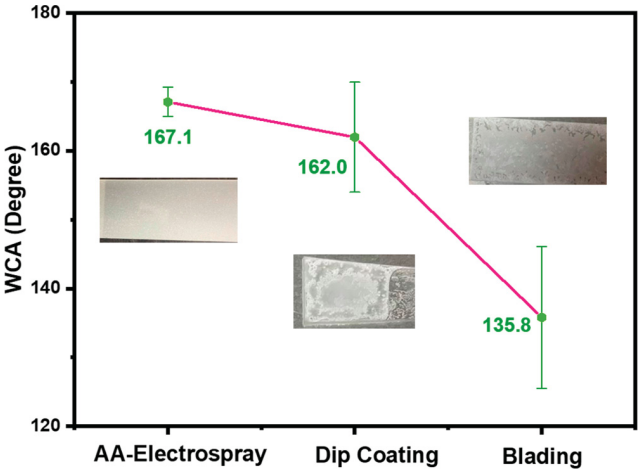

Figure 2. Comparison of three methods: air-assisted electrospray (AA-electrospray), dip coating, and blading.

in the highest WCA of 167.1° with the smallest standard deviation. The WCA of 167.1° was obtained at 200 mg of SiO_2, 50 mg of PAN, 1 h of spraying time, 20 kV of power supply, 30 μL/min solution infused rate, and 3 L/min air flow rate. The electrosprayed sample also shows excellent uniformity of the coating on the glass substrate. A superhydrophobic surface is also obtained by the dip coating method; however, after it was allowed to dry in air, the coating cracked which affected the uniformity of the material distribution. Blading does not achieve the superhydrophobic property, as shown in the WCA measurement of 135.8° with a very large standard deviation due to cracking occurring on the surface. Hence, air-assisted electrospraying is highly advantageous for the facile fabrication of a superhydrophobic coating. Moreover, large surface area deposition can be achieved by a multinozzle system and adjusted by nozzle number. The thickness of the deposited layer and loading can be controlled by the time variable.[24] In the following sections, various parameters will be studied for better understanding of the system.

3.2. Effect of SiO_2 Nanoparticles. In the experimental design, SiO_2 is used to control the surface roughness. Various amounts of SiO_2 nanoparticles in the spray solution, including 50, 150, 200, and 250 mg, were used to study the effect of SiO_2 on the wettability of coated surfaces. For simplicity, the

https://doi.org/10.1021/acs.langmuir.1c03134
Langmuir 2022, 38, 2852−2861

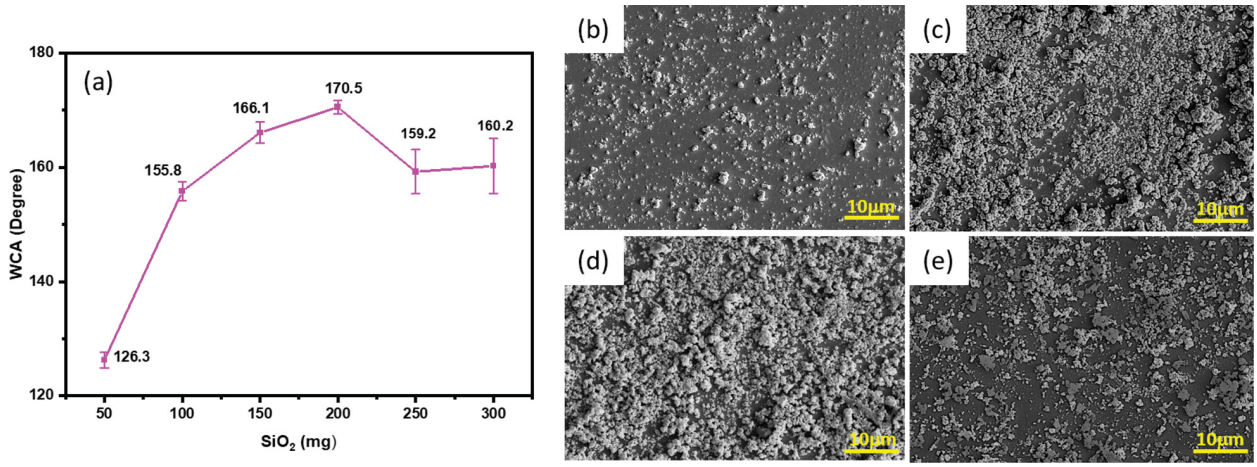

Figure 3. Effect of SiO_2 nanoparticles. (a) Water contact angle (WCA) versus amount of SiO_2 nanoparticles in the sprayed solution. Each data point represents $n = 5$ measurements, and the lower and upper error values represent the minimum and maximum measured values, respectively. (b–e) SEM images of (b) SO-50, (c) SO-150, (d) SO-200, and (e) SO-250.

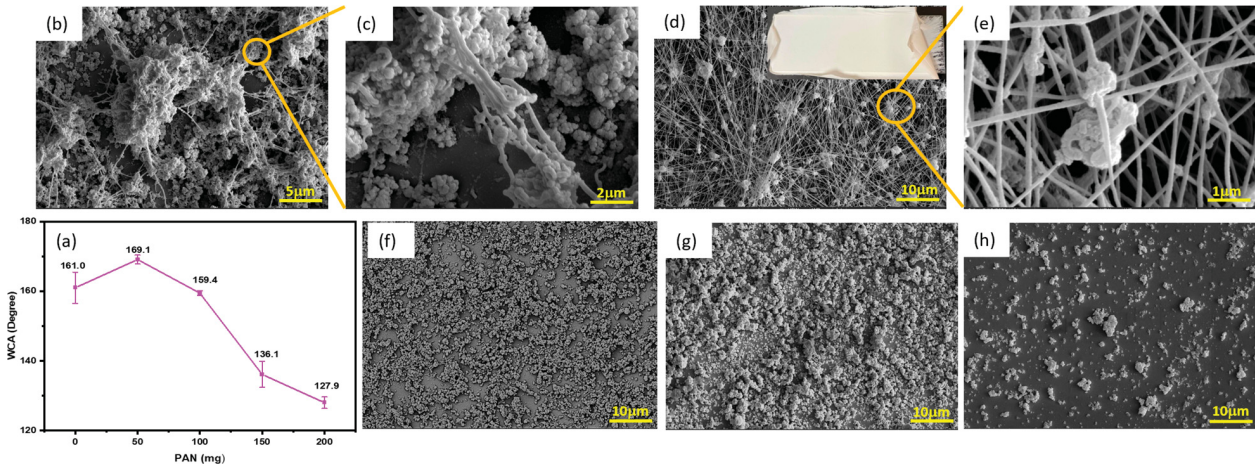

Figure 4. Effect of PAN. (a) Relationship between WCAs of coated surfaces at various amounts of PAN in sprayed solutions. (b–d) SEM images of sample after electrospraying of (b, c) 50 and (d, e) 200 mg of PAN. The inset image in (d) shows fiber layer peeling off the glass's surface. (f–h) SEM images of sample after completing fabrication process (annealing and CVD) of (f) 0, (g) 50, and (h) 200 mg of PAN.

surfaces are denoted as SO-50, SO-150, SO-200, and SO-250, respectively. Each WCA data point represents the average of five measurements at different locations of the samples. The WCA data and SEM images, as shown in Figure 3, confirm that the amount of SiO_2 nanopowder significantly affects the superhydrophobicities and morphologies of the coatings. The water droplet at SO-50 shows a low contact angle where the surface's superhydrophobicity is not obtained. The SEM image of this sample (Figure 3b) confirms the coating after heat treatment is inadequate to cover a whole surface. Therefore, the roughness level of this sample is too low to obtain a superhydrophobic surface. At 100 mg of SiO_2, the coated surfaces begin to achieve superhydrophobic properties, where the WCA is greater than 150°. The WCA increases as the amount of SiO_2 increases until it obtains the highest measurement of 170.5° at SO-200. After SO-200, the WCA decreases but still maintains superhydrophobicity. A small error bar at a data point represents the uniform distribution of the coating, whereas a large error bar indicates a higher variation in WCA measurements at different spots of the coating. The error bar illustration shows that, at less than SO-200, electrospray results in uniform coating distribution. After SO-200, the sprayed solution was deposited unevenly on the surfaces, resulting in a higher gap between the minimum and maximum measured values at the same sample. From the SEM images in Figure 3, the coating is getting denser as the amount of SiO_2 increases from SO-150 to SO-200. Compared to SO-200, SO-250 has less coating on the surface, possibly due to lower adhesion between the coating and substrate at SO-250. Therefore, most parts of the coating are easily removed after annealing at 600 °C in air. It is concluded that 200 mg is the optimal amount of SiO_2 which can result in very good coverage and the highest WCA.

3.3. Effect of Polyacrylonitrile (PAN). PAN in the solution serves two purposes. One is to increase the viscosity and help SiO_2 disperse well in the precursor solution rather than precipitate out; the other is to better guide the droplet spray and for better adhesion on the substrate. As shown in Figure 4, the WCA of solution without PAN is 161.0°. With the presence of 50 mg of PAN in the sprayed solution, the superhydrophobicity of the coating increases, demonstrated by its WCA of 169.1°. Even though the CA measurements do not show significant differences when a small amount of PAN is added, the distribution of coating on the substrate's surface is

https://doi.org/10.1021/acs.langmuir.1c03134
Langmuir 2022, 38, 2852–2861

more even, which is confirmed by the magnitude of the standard deviations of 0 and 50 mg PAN samples. Increasing the amount of PAN is expected to increase the superhydrophobic behavior of the coatings. However, WCA data starts decreasing dramatically after the addition of more PAN in the solution. The wettability of the coating changes from superhydrophobic to hydrophobic when the amount of PAN increases to 150 mg. At 200 mg of PAN, the coating no longer obtains antiwetting behavior in which its CA is 127.9°.

Figure 4b–e show the SEM images of the coating after electrospraying. At this stage, thermal treatment has not yet been applied to the coating. In a comparison of the SEM images at 50 mg of PAN (Figure 4b,c) and the images at 200 mg of PAN (Figure 4d,e), the higher amount of PAN results in a denser fiber structure. As seen in the magnified SEM image of Figure 4c, the deposited layers possess few fibers among SiO_2 depositions, whereas the fiber structure prevails in Figure 4e. When the coating becomes fibrous, it easily peels off the surface which leads to low adhesion, shown in the inset image of Figure 4d. After heat treatment at high temperature (600 °C), PAN in the coating is burned out. Therefore, the distribution of the spray on the surface with high amounts of PAN (e.g., 150 and 200 mg of PAN) is uneven, which results in a higher standard deviation in WCA measurements on different locations of the surface. Parts f, g, and h of Figure 4 represent the surfaces after completion of the fabrication process at 0, 50, and 200 mg of PAN, respectively. From the coating density comparison, 50 mg of PAN results in better coverage and the best superhydrophobic behavior. In addition, the coating is wiped off significantly at 200 mg of PAN after the thermal process.

3.4. Effect of Solution Infused Rate. At the same materials' concentration, the relationship between the WCA and the solution infused rate, from 10 to 50 μL/min, is shown in Figure 5a. With the increasing solution infused rate, the water contact angles first increase and then decrease. When the infused rate is 30 μL/min, the WCA reaches the maximum value of 172.5°, so the solution infused rate for the air-assisted electrospray process is selected to be 30 μL/min. With the increase of the infused rate, the coating on the substrate was generated to be thicker, resulting in a denser micro/nano rough structure. This rough structure, shown in Figure 5c, is more uniform than the structure at the solution infused rate of 10 μL/min (Figure 5b). The WCA starts decreasing significantly at infused rates higher than 40 μL/min; however, the surface's superhydrophobicity is still maintained. Figure 5d is the SEM image of the surface at 50 μL/min. When the infused rate is too high, the center area of the surface is wetted, as described in the inset image of Figure 5d. This wetted area, after the annealing process at 600 °C for 1 h, leaves a thinner layer of the coating comparing to the outer area which is not wetted during spraying, indicating the simultaneous evaporation of solvent is crucial for coating uniformity and structure control. Thus, the superhydrophobicity decreases due to the reduction in coating thickness after annealing of the wetted spot of the surface.

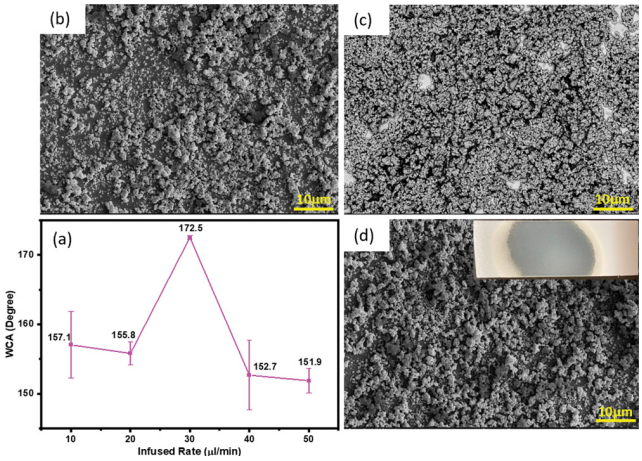

Figure 5. Effect of solution infused rate. (a) WCAs of coated layers on glass substrates at different solution infused rates. (b–d) SEM images of coated surface for solution infused rate at (b) 10, (c) 30, and (d) 50 μL/min. Inset image in (d) of wetting spot of coated surface after electrospraying at the infused rate of 50 μL/min.

3.5. Effect of Sprayed Voltage. To evaluate the effect of voltage on the superhydrophobicity of the coatings, different voltage conditions were examined, as shown in Figure 6a. The voltages used were 0, 5, 10, 15, and 20 kV. SEM images in Figure 6b–d represent the morphology of coating when there is no power supply (0 kV) and when it is at 10 and 20 kV, respectively. Three distinct phenomena were observed. When there is no voltage, the solution is sprayed toward one focused circular section, as seen in Figure 6b. This condition obtains an average WCA of 145.6° with a remarkable standard deviation. After five measurements on different locations of the coated surface, the maximum WCA is 154.54° and the minimum WCA is 136.66°. The maximum WCA is obtained when measuring inside the circular area. The minimum WCA is measured in the outer shell where a only small amount of solution is reached. As the voltage increases to 10 kV (Figure 6c), the coating starts spreading more on the surface instead of focusing on one area, which results in a higher WCA of 158.5°. However, the distribution of the coating is still uneven. The coating at the 20 kV condition is denser (Figure 6d). Figure 6e,f shows magnified SEM images of the coated layer at 20 kV. From the thickness and distribution comparison, it is clear that higher voltage results in a higher WCA measurement. If the safety factor is neglected, a WCA higher than 167.8° could be hypothetically achieved in continuaton of experimentation with voltage higher than 20 kV. The higher working voltage represents a higher electrostatic force for the charged droplets. The results indicate the electrostatic force is critical for the coating distribution and quality, serving as a critical driving force to impact droplets' displacement on the substrates.

3.6. Effect of Sprayed Time. Various spraying periods were selected to study the effect of surface modification on the surface wetting behavior. Figure 7a shows the WCA values in relation to the sprayed periods. The graph does not show significant differences in CA values at different times. All the samples result in hydrophobic surfaces, in which the WCA is greater than 150°. Parts b, c, and d of Figure 7 represent the surface morphology of the coating at 15 min, 1 h, and 2 h of spraying, respectively. SEM images show that all samples have similar structures of small piles of particles packed on top of each other with voids in between. These structures create the adequate roughness for the surface to trap air and reduce the solid–liquid contact area. The superhydrophobic behavior can be achieved in the short period of spray time, as evidenced by the fact that 15 min results in a WCA measurement similar to that at 2.5 h. Therefore, it is unnecessary to run the electrospraying process for a long time since there is not

https://doi.org/10.1021/acs.langmuir.1c03134
Langmuir 2022, 38, 2852–2861

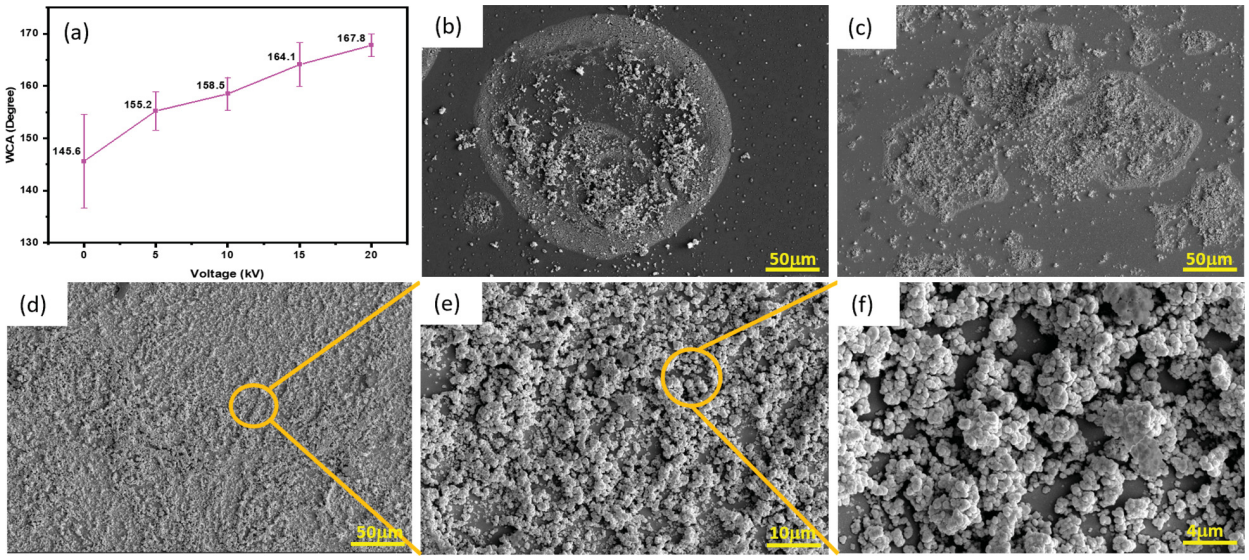

Figure 6. Effect of sprayed voltage. (a) WCA and sprayed voltage relationship. (b–f) SEM images of coated surfaces at sprayed voltages of (b) 0, (c) 10, and (d–f) 20 kV.

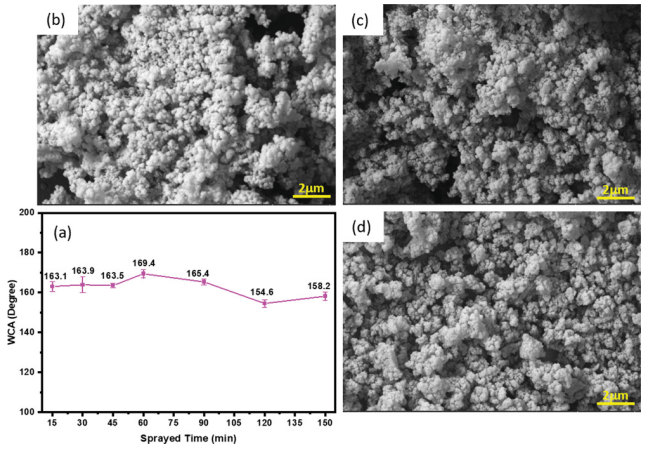

Figure 7. Effect of sprayed time. (a) Relationship between WCA and sprayed time on superhydrophobic performances. (b–d) SEM images of coated surfaces at sprayed times of (b) 15 min, (c) 1 h, and (d) 2 h.

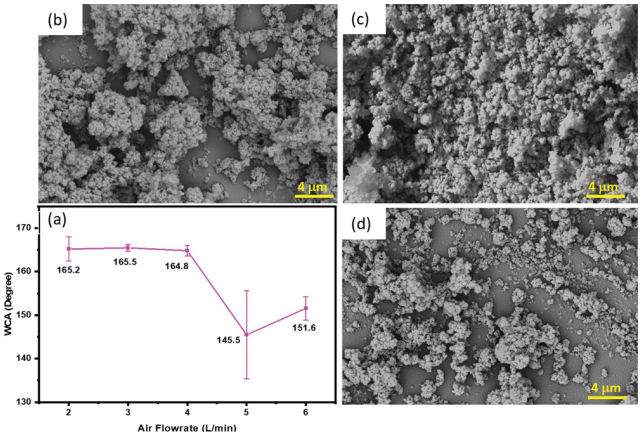

Figure 8. Effect of air flow rate. (a) Relationship between WCA and sprayed time on superhydrophobic performances. (b–d) SEM images of coated surfaces at air flow rates of (b) 2, (c) 3, and (d) 5 L/min.

much difference in surface morphology between the spray times. It is concluded that, once enough coverage is achieved, the extended spray time will not make a significant impact on the surface structure and WCA. According to this set of experiments, the 1 h experiment results in the highest WCA value of 169.4°. The 1 h spraying period was determined to spray the coating that combines all the optimal factors in this study.

3.7. Effect of Air Flow Rate. To better understand the effect of air flow of electrospray deposition on the superhydrophobic coating, WCAs were determined at various air flow rates of 2, 3, 4, 5, and 6 L/min. The relationship between WCA and air flow is shown in Figure 8a. The coating maintains its superhydrophobic property when the air flow rate is less than 4 L/min. The higher air flow results in random solution direction deposited on the glass substrate; thus it leads to a lower WCA with a larger standard deviation of the coating distribution. The most superhydrophobic and uniform layer is achieved at the air flow rate of 3 L/min. At this air flow rate, the coating obtains a dense rough structure, as shown in the SEM image of Figure 8c. Compared to the coating at the air flow rate of 3 L/min, the air flow rate of 2 L/min results in a similar roughness but less uniform structure (Figure 8b). The SEM image of the coating at the air flow rate of 5 L/min (Figure 8d) shows a significant reduction in rough structure as well as uniformity, because the force of air flow now dominates the particle movement and direction rather the electrostatic forces. It also indicates that the balance of electrostatic force and air force is very crucial. Therefore, the selected air flow rate for the air-assisted electrospray deposition is 3 L/min.

3.8. Coating with Optimal Factors Combination and Other Properties. To verify whether the parameters always have a positive interaction effect, the superhydrophobic coating was prepared by using the combination of the optimal solution concentrations and air-assisted electrospray parameters identified above. As discussed in previous sections, these parameters are chosen to be 50 mg of PAN and 200 mg of SiO_2 in DMF solution, 20 kV power supply, 30 μL/min solution infused rate, and 3 L/min air flow rate. The prepared coating obtains the static contact angle of 167.1°, which is superhydrophobic, whereas the pristine borosilicate glass

https://doi.org/10.1021/acs.langmuir.1c03134
Langmuir 2022, 38, 2852−2861

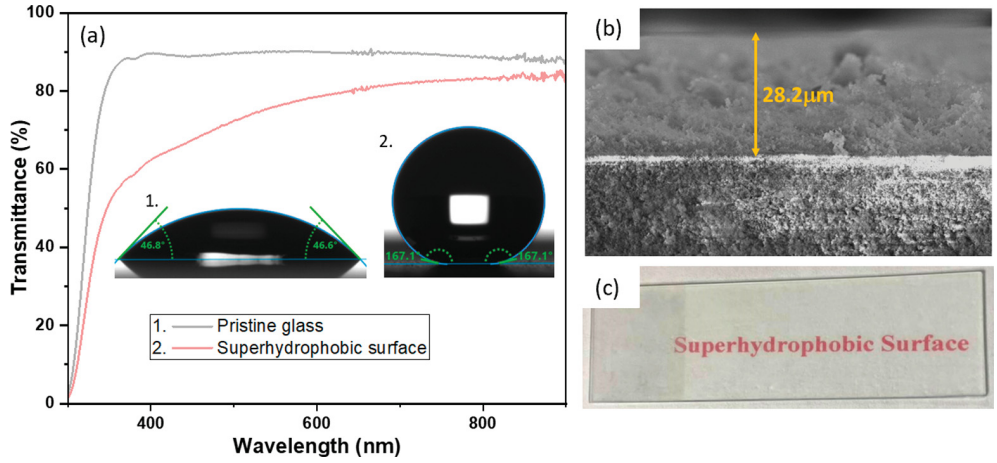

Figure 9. Properties of the superhydrophobic surface. (a) Ultraviolet−visible transmittance spectra of superhydrophobic surface compared to pristine glass. The inset images show a water droplet with its static contact angle on a pristine glass and on superhydrophobic surface. (b) Cross-sectional SEM image of coated glass substrate. (c) Photograph showing transparency of the printed text behind the glass slide covered with superhydrophobic coating.

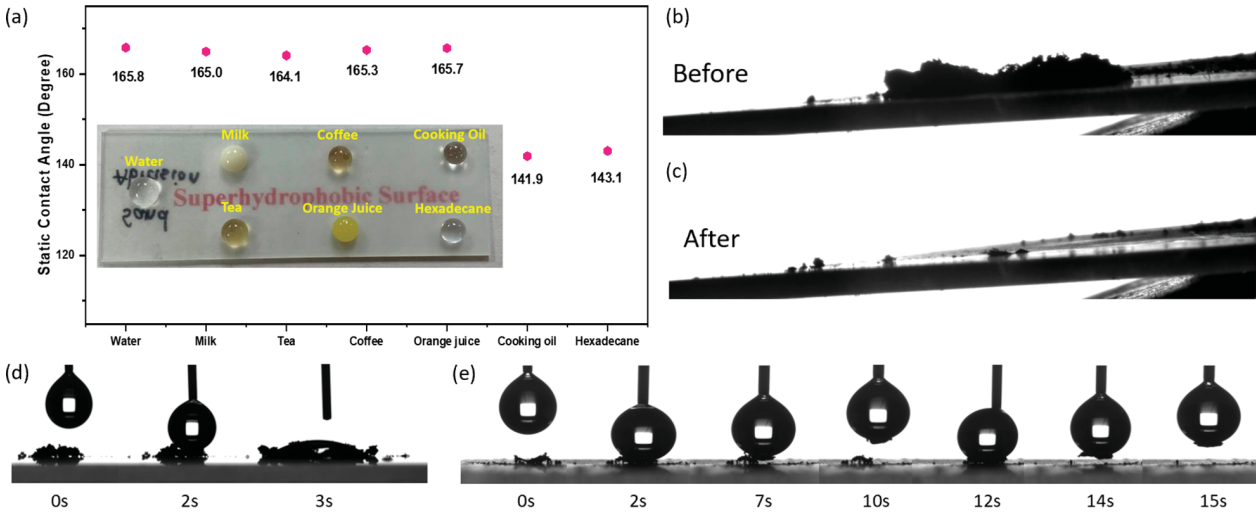

Figure 10. Application of superhydrophobic surface. (a) Static contact angles of different liquids on prepared superhydrophobic substrate. The inset image is a photograph of different liquids on the coated surface. (b, c) Images of carbon black particles on the coated surface (b) before and (c) after dropping of multiple water droplets on the surface. These images were captured by the contact angle measurement instrument. (d, e) Time-resolved images of carbon black picking up 6 μL water droplet on (d) uncoated glass substrate and (e) the superhydrophobic surface.

contact angle is 46.8°, which is completely wetted. It is also noted the obtained contact angle with the selected parameters is close to but not the highest number in this study, indicating that not all factors interfere in a positive way. In addition, the coated surface before CVD of trichloro(1*H*,1*H*,2*H*,2*H*-perfluorooctyl)silane is completely wetted during the water drop test, whereas it exhibits the superhydrophobic property after CVD. A superhydrophobic surface can be successfully achieved only if two main criteria are met, which are rough structure and low surface energy. SiO_2/PAN solution was fabricated on a glass surface through the air-assisted electrospray method and then was cured at high temperature to create a rough structure. Since SiO_2 is hydrophilic, the rough structure remains hydrophilic which results in a completely wetted surface. Trichloro(1*H*,1*H*,2*H*,2*H*-perfluorooctyl)silane is a low-surface-energy material; therefore, the coated surface after CVD obtains both rough structure and low surface energy, which results in a superhydrophobic surface. Without the SiO_2 rough structure, the trichloro(1*H*,1*H*,2*H*,2*H*-perfluorooctyl)silane coated glass has a contact angle of 105.53°. The coating thickness was found to be 28.2 μm (Figure 9b). The transparency and superhydrophobicity are mutually exclusive, which means higher rough structure leads to light scattering and, thus, it reduces the transparency.[3] In this study, the transmittance percentage is determined to evaluate the transparency of the surface. The transmittance spectra of the superhydrophobic surface and a pristine glass are demonstrated in Figure 9a. For wavelengths above 500 nm, the transmittance of superhydrophobic surface in this study is above 60%, which is reduced by less than 30% as compared to that of pristine glass. Even with the reduction in transmittance compared to the pristine glass, this transparency of the prepared superhydrophobic surface is still well reflected in the easy readability of letters underneath the coated glass substrate (Figure 9c). Thickness control and more ordered nanostructures will be explored as a continuing effort to increase transparency so that the application can be extended to electronic screens.

https://doi.org/10.1021/acs.langmuir.1c03134
Langmuir 2022, 38, 2852−2861

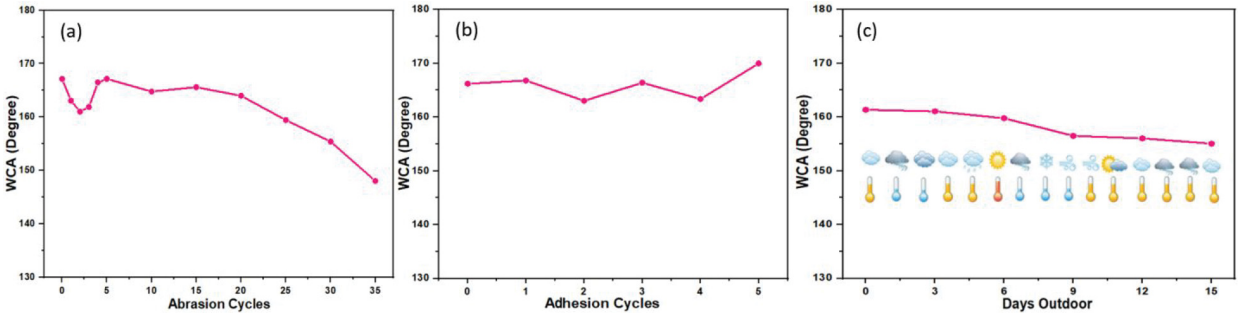

Figure 11. Reliability of the coated layer. WCAs measured after (a) sandpaper abrasion, (b) adhesion cycles, and (c) outdoor exposure examination on the as-prepared surface.

3.9. Applications. The prepared superhydrophobic surface shows remarkable performance on super-repelling common water solutions, such as milk, coffee, tea, and orange juice. In addition, low wetting behavior with extremely nonpolar liquids, such as cooking oil and hexadecane, is demonstrated in Figure 10a. The droplets of all the liquids did not wet the surface, and they exhibit typical spherical shapes. The water solutions obtained static contact angles above 164°, which well demonstrate super-repellency. Cooking oil and hexadecane exhibit static contact angles above 141°, which represents low wetting behavior. The coated superhydrophobic surface is nonpolar. Water is polar, while cooking oil and hexadecane are nonpolar. Therefore, nonpolar cooking oil/hexadecane molecules tend to have more interaction with the nonpolar superhydrophobic surface, which results in the inferior wetting behavior of the surface toward cooking oil and hexadecane compared to water-based solution. The self-cleaning functionality of the coatings was experimented with 1 mg carbon black particles deposited on the coated surface. Multiple droplets were injected and rolled off of the surface which was placed at an angle of 20° from the flat table surface. As seen in Figure 10b,c, carbon black particles were significantly removed after deposition of water droplets on the surface, which well-highlighted its self-cleaning functionality. Parts d and e of Figure 10 are time-resolved images of a 6 μL water droplet depositing on a small amount carbon black particles on a pristine glass and the superhydrophobic surface. As seen in Figure 10d, the surface is rapidly wetted after dropping of water on the pristine glass surface, showing no self-cleaning capability. On the other hand, the water droplet remains attached to the needle after injection to the superhydrophobic surface (Figure 10e), which demonstrates the significantly low surface tension of the coating. Therefore, the water droplet was able to be lifted up from the superhydrophobic surface with carbon black particles as the needle moved up. After two lifting cycles, there was no carbon black particle left on the surface, which represents the good self-cleaning functionality of the prepared coating.

3.10. Reliability of the Coated Layer. Abrasion examination is one of the universal methods used for evaluating the durability of a superhydrophobic surface against the physical force.[8,30,31] In this study, sandpaper abrasion was performed to demonstrate the reliability of the superhydrophobic coating in different harsh environmental conditions. The WCAs of the coated glass slide before and after abrasion cycles are shown in Figure 11a. The WCA of the as-prepared glass slide is 167.2°. The WCA decreases in the first three abrasion cycles, and then it starts increasing and reaches 167.2° at the fifth cycle. Afterward, the WCA slightly decreases as abrasion cycle increases. The thick coating layer of 28.2 μm (Figure 9b) results in lower adhesion of the top particle, namely, more loose structure. Thus, the top loose particles of the coating were first removed in the first three sandpaper abrasion cycles while the rough structure was maintained. Five abrasion cycles exhibit a thinner coated layer with better adhesive force to the glass substrate, thus resulting in increasing the WCA to 167.2°. Thus, the coated layer possesses better transparency, but its structure remains as rough as it was before abrasion. This result indicates a thinner coating with the same superhydrophobicity is possible. Even though the WCA slightly decreased after the fifth cycle, the coated glass slide retained its strong water repellent characteristics after 30 abrasion cycles, displaying good mechanical robustness. In addition, the tape adhesion test was considered to study the mechanical robustness of the as-prepared superhydrophobic coating. Subsequently a 3M double-sided tape was harshly pressed onto the coated surface, scratched, held for 10 s, and torn off. The relationships between the WCA and peeling cycles are demonstrated in Figure 11b. The coating retains its superhydrophobicity during the tested peeling cycles.

The durability of the superhydrophobic coating against strong acid and base environments was also studied in this paper. The coated layer appeared to remain the same with no peeling after interacting with acid and base solution. The WCA measurements did not fluctuate significantly after acid and base examination, which leads to the conclusion that the superhydrophobic surface has excellent antiacid and antibase capability. Before acid/base testing, the two coated surfaces obtained WCAs of 154.79 ± 1.30° and 153.45 ± 0.95°. After immersion in acid/base solution, the WCAs of the two coatings were 156.94 ± 1.21° and 152.9 ± 4.87° in acid and base solutions, respectively. An additional experiment to rinse off the coated surface with DI water after acid/base tests followed by drying in air at room temperature was studied. The coating remained with strong adhesion on the glass substrate with no peeling off. The WCA measurements in this case were similar to the one without rinsing with DI water. Therefore, rinsing off with water did not affect the durability of the surface or the superhydrophobic property.

An outdoor exposure examination was done to determine the durability of the coated superhydrophobic surface. The humidity within 15 days drastically varied between 39 and 93%. The temperature ranged from 37 to 72 °F. The weather conditions were quite diverse, such as cloudy, windy, breezy, clear, calm, sunny, and light rainy. Water contact angle

https://doi.org/10.1021/acs.langmuir.1c03134
Langmuir 2022, 38, 2852−2861

measurements of the coated surface for outdoor exposure experiment are presented in Figure 11c. The surface retained its superhydrophobic property throughout the diversity of weather conditions. The WCAs of the coated glass slide were 161.35 and 155.05° before and after 15 days of exposure to the outdoor environment. As a result, the mechanical robustness of the coating withstands well a variety of weather climates.

4. CONCLUSION

In summary, this study presented a facile air-assisted electrospray technique to prepare a self-cleaning superhydrophobic surface. The influences of coating precursor compositions and spraying conditions on the surface properties were thoroughly analyzed. The coated surface exhibited remarkable water and oil repellent characteristic as well as good robustness toward harsh physical and chemical conditions. Furthermore, the coatings showed an excellent self-cleaning performance. Thus, this simple and straightforward method represents an important technique addition to the current field of self-cleaning coatings for various potential engineering and daily use applications.

AUTHOR INFORMATION

Corresponding Author

Ling Fei − *Department of Chemical Engineering, Institute for Materials Research and Innovation, University of Louisiana at Lafayette, Lafayette, Louisiana 70504, United States;* orcid.org/0000-0002-0954-5168; Email: ling.fei@louisiana.edu

Authors

Thu Nguyen − *Department of Chemical Engineering, Institute for Materials Research and Innovation, University of Louisiana at Lafayette, Lafayette, Louisiana 70504, United States*

Philip Wortman − *Department of Petroleum Engineering, University of Louisiana at Lafayette, Lafayette, Louisiana 70504, United States*

Zizhou He − *Department of Chemical Engineering, Institute for Materials Research and Innovation, University of Louisiana at Lafayette, Lafayette, Louisiana 70504, United States*

Joshua Goulas − *Department of Chemical Engineering, Institute for Materials Research and Innovation, University of Louisiana at Lafayette, Lafayette, Louisiana 70504, United States*

Hui Yan − *Department of Chemistry, University of Louisiana at Lafayette, Lafayette, Louisiana 70504, United States;* orcid.org/0000-0001-9279-5370

Mehdi Mokhtari − *Department of Petroleum Engineering, University of Louisiana at Lafayette, Lafayette, Louisiana 70504, United States*

Xiao-Dong Zhou − *Department of Chemical Engineering, Institute for Materials Research and Innovation, University of Louisiana at Lafayette, Lafayette, Louisiana 70504, United States*

Complete contact information is available at: https://pubs.acs.org/10.1021/acs.langmuir.1c03134

Notes

The authors declare no competing financial interest.

ACKNOWLEDGMENTS

This research is funded by the Louisiana Transportation Research Center under No. DOTLT1000417 and NASA under 80NSSC21M0333. We also acknowledge facility support from the NSF MRI Program (NSF-1920166).

REFERENCES

(1) Li, W.; Amirfazli, A. Microtextured Superhydrophobic Surfaces: A Thermodynamic Analysis. *Adv. Colloid Interface Sci.* **2007**, *132* (2), 51−68.

(2) Milne, A. J. B.; Amirfazli, A. The Cassie Equation: How It Is Meant to Be Used. *Adv. Colloid Interface Sci.* **2012**, *170* (1−2), 48−55.

(3) Fei, L.; He, Z.; LaCoste, J. D.; Nguyen, T. H.; Sun, Y. A Mini Review on Superhydrophobic and Transparent Surfaces. *Chem. Rec.* **2020**, *20* (11), 1257−1268.

(4) Li, Y.; Zhang, R.; Yu, H.; Chen, G.; Zhu, M.; Qiu, B.; Zou, H.; Li, X. Fluorinated Nanosilica Size Effect on Hierarchical Structure and Superhydrophobic Properties of the Epoxy Nanocomposite Film. *ACS Appl. Polym. Mater.* **2020**, *2* (2), 418−426.

(5) Butt, H. J.; Roisman, I. V.; Brinkmann, M.; Papadopoulos, P.; Vollmer, D.; Semprebon, C. Characterization of Super Liquid-Repellent Surfaces. *Curr. Opin. Colloid Interface Sci.* **2014**, *19* (4), 343−354.

(6) Xue, C. H.; Guo, X. J.; Ma, J. Z.; Jia, S. T. Fabrication of Robust and Antifouling Superhydrophobic Surfaces via Surface-Initiated Atom Transfer Radical Polymerization. *ACS Appl. Mater. Interfaces* **2015**, *7* (15), 8251−8259.

(7) Xue, Z.; Wang, S.; Lin, L.; Chen, L.; Liu, M.; Feng, L.; Jiang, L. A Novel Superhydrophilic and Underwater Superoleophobic Hydrogel-Coated Mesh for Oil/Water Separation. *Adv. Mater.* **2011**, *23* (37), 4270−4273.

(8) Huang, J.; Yang, M.; Zhang, H.; Zhu, J. Solvent-Free Fabrication of Robust Superhydrophobic Powder Coatings. *ACS Appl. Mater. Interfaces* **2021**, *13* (1), 1323−1332.

(9) Jeon, Y.; Nagappan, S.; Li, X. H.; Lee, J. H.; Shi, L.; Yuan, S.; Lee, W. K.; Ha, C. S. Highly Transparent, Robust Hydrophobic, and Amphiphilic Organic-Inorganic Hybrid Coatings for Antifogging and Antibacterial Applications. *ACS Appl. Mater. Interfaces* **2021**, *13* (5), 6615−6630.

(10) Nundy, S.; Ghosh, A.; Mallick, T. K. Hydrophilic and Superhydrophilic Self-Cleaning Coatings by Morphologically Varying ZnO Microstructures for Photovoltaic and Glazing Applications. *ACS Omega* **2020**, *5* (2), 1033−1039.

(11) Bayer, I. S. On the Durability and Wear Resistance of Transparent Superhydrophobic Coatings. *Coatings* **2017**, *7* (1), 12.

(12) Doganci, M. D. Fabrication of Superhydrophobic Transparent Cyclic Olefin Copolymer (COC)-SiO2 Nanocomposite Surfaces. *J. Appl. Polym. Sci.* **2021**, *138* (14), 50145.

(13) Manifar, T.; Rezaee, A.; Sheikhzadeh, M.; Mittler, S. Formation of Uniform Self-Assembly Monolayers by Choosing the Right Solvent: OTS on Silicon Wafer, a Case Study. *Appl. Surf. Sci.* **2008**, *254* (15), 4611−4619.

(14) Siddiqui, A. R.; Li, W.; Wang, F.; Ou, J.; Amirfazli, A. One-Step Fabrication of Transparent Superhydrophobic Surface. *Appl. Surf. Sci.* **2021**, *542*, 148534.

(15) Janowicz, N. J.; Li, H.; Heale, F. L.; Parkin, I. P.; Papakonstantinou, I.; Tiwari, M. K.; Carmalt, C. J. Fluorine-Free Transparent Superhydrophobic Nanocomposite Coatings from Mesoporous Silica. *Langmuir* **2020**, *36* (45), 13426−13438.

(16) Zhao, S.; Zhao, J.; Wen, M.; Yao, M.; Wang, F.; Huang, F.; Zhang, Q.; Cheng, Y. B.; Zhong, J. Sequentially Reinforced Additive Coating for Transparent and Durable Superhydrophobic Glass. *Langmuir* **2018**, *34* (38), 11316−11324.

(17) Zheng, H.; Pan, M.; Wen, J.; Yuan, J.; Zhu, L.; Yu, H. Robust, Transparent, and Superhydrophobic Coating Fabricated with Waterborne Polyurethane and Inorganic Nanoparticle Composites. *Ind. Eng. Chem. Res.* **2019**, *58* (19), 8050−8060.

(18) Teshima, K.; Sugimura, H.; Inoue, Y.; Takai, O.; Takano, A. Transparent Ultra Water-Repellent Poly(Ethylene Terephthalate) Substrates Fabricated by Oxygen Plasma Treatment and Subsequent Hydrophobic Coating. *Appl. Surf. Sci.* **2005**, *244* (1−4), 619−622.
(19) Hao, L.; Gao, T.; Xu, W.; Wang, X.; Yang, S.; Liu, X. Preparation of Crosslinked Polysiloxane/SiO 2 Nanocomposite via in-Situ Condensation and Its Surface Modification on Cotton Fabrics. *Appl. Surf. Sci.* **2016**, *371*, 281−288.
(20) Zhu, X.; Zhang, Z.; Ren, G.; Men, X.; Ge, B.; Zhou, X. Designing Transparent Superamphiphobic Coatings Directed by Carbon Nanotubes. *J. Colloid Interface Sci.* **2014**, *421*, 141−145.
(21) Kim, M.; Kim, K.; Lee, N. Y.; Shin, K.; Kim, Y. S. A Simple Fabrication Route to a Highly Transparent Super-Hydrophobic Surface with a Poly(Dimethylsiloxane) Coated Flexible Mold. *Chem. Commun.* **2007**, *22*, 2237−2239.
(22) Cavalli, A.; Mugele, F. Superamphiphobic Surfaces. In *Droplet Wetting and Evaporation*; Brutin, D., Ed.; Elsevier Inc.: 2015; p 57..
(23) Chen, C.; Weng, D.; Chen, S.; Mahmood, A.; Wang, J. Development of Durable, Fluorine-Free, and Transparent Superhydrophobic Surfaces for Oil/Water Separation. *ACS Omega* **2019**, *4* (4), 6947−6954.
(24) Fei, L.; Yoo, S. H.; Villamayor, R. A. R.; Williams, B. P.; Gong, S. Y.; Park, S.; Shin, K.; Joo, Y. L. Graphene Oxide Involved Air-Controlled Electrospray for Uniform, Fast, Instantly Dry, and Binder-Free Electrode Fabrication. *ACS Appl. Mater. Interfaces* **2017**, *9* (11), 9738−9746.
(25) Lee, J. H.; Kang, J.; Kim, S. W.; Halim, W.; Frey, M. W.; Joo, Y. L. Effective Suppression of the Polysulfide Shuttle Effect in Lithium-Sulfur Batteries by Implementing RGO-PEDOT:PSS-Coated Separators via Air-Controlled Electrospray. *ACS Omega* **2018**, *3* (12), 16465−16471.
(26) Heo, K. J.; Oh, H. J.; Eom, H.; Kim, Y.; Jung, J. H. High-Performance Bag Filter with a Super-Hydrophobic Microporous Polytetrafluoroethylene Layer Fabricated by Air-Assisted Electrospraying. *Sci. Total Environ.* **2021**, *783*, 147043.
(27) Niknejad, A. S.; Bazgir, S.; Kargari, A.; Barani, M.; Ranjbari, E.; Rasouli, M. A High-Flux Polystyrene-Reinforced Styrene-Acrylonitrile/Polyacrylonitrile Nanofibrous Membrane for Desalination Using Direct Contact Membrane Distillation. *J. Membr. Sci.* **2021**, *638*, 119744.
(28) Lee, J.; Ko, B.; Kang, J.; Chung, Y.; Kim, Y.; Halim, W.; Lee, J. H.; Joo, Y. L. Facile and Scalable Fabrication of Highly Loaded Sulfur Cathodes and Lithium−Sulfur Pouch Cells via Air-Controlled Electrospray. *Mater. Today Energy* **2017**, *6*, 255−263.
(29) Halim, W.; Lee, J. H.; Park, S. M.; Zhang, R.; Sarkar, S.; O'Neil, T.; Chiang, Y. C.; Joo, Y. L. Directly Deposited Binder-Free Sulfur Electrode Enabled by Air-Controlled Electrospray Process. *ACS Appl. Energy Mater.* **2019**, *2* (1), 678−686.
(30) She, Z.; Li, Q.; Wang, Z.; Li, L.; Chen, F.; Zhou, J. Researching the Fabrication of Anticorrosion Superhydrophobic Surface on Magnesium Alloy and Its Mechanical Stability and Durability. *Chem. Eng. J.* **2013**, *228*, 415−424.
(31) Liu, M.; Li, J.; Hou, Y.; Guo, Z. Inorganic Adhesives for Robust Superwetting Surfaces. *ACS Nano* **2017**, *11* (1), 1113−1119.

https://doi.org/10.1021/acs.langmuir.1c03134
Langmuir 2022, 38, 2852−2861